Materiales de Construcción 75 (359)
July-September 2025, e389
ISSN-L: 0465-2746
https://doi.org/10.3989/mc.2025.388224

Experimental study on mechanical properties and microscopic analysis of basalt-polypropylene hybrid fiber reinforced concrete

Y. Huang[a], H. Liu[a], G. Liu[b] ✉

a. School of Civil and Architectural Engineering, Liaoning University of Technology, (Jinzhou, China)
b. Lecturer, School of Civil Engineering, Ningbo Tech University, (Ningbo, China)
✉: liugenjin@163.com

Received 19 June 2024
Accepted 10 March 2025
Available on line 17 March 2026

ABSTRACT: In this paper, the effects of basalt fiber aspect ratio (BFA), basalt fiber content (BFC) and polypropylene fiber content (PFC) on the basic mechanical properties of basalt-polypropylene hybrid fiber reinforced concrete (BPHFRC) were studied by orthogonal test. Furthermore, the failure mode of concrete were examined by scanning electron microscope (SEM). The results show that mixing BF and PF leads to a positive hybrid effect, and the impact of BFC is the most significant. The cubic compressive and axial compressive strengths decrease with increased BFC. The combination of A2B1C2 (BFA=800, BFC=0.1%, PFC=0.15%) increased the cubic compressive and axial compressive strengths by 13.73% and 23.54%, respectively. The combination of A2B2C3 (BFA=800, BFC=0.15%, PFC=0.2%) increased the splitting tensile and flexural strengths by 32.96% and 38.88%. The strength prediction models are reliable. SEM observed that fiber bridging prevented crack initiation and growth.

KEY WORDS: Basalt fiber; Polypropylene fiber; Hybrid fiber; Mechanical properties; Microstructure analysis.

Citation/Citar como: Huang Y, Liu H, Liu G. 2025. Experimental study on mechanical properties and microscopic analysis of basalt-polypropylene hybrid fiber reinforced concrete. Mater. Construcc. 75(359):e389. https://doi.org/10.3989/mc.2025.388224

RESUMEN: *Estudio experimental de las propiedades mecánicas y análisis microscópico del hormigón reforzado con fibras híbridas de basalto-polipropileno.* En este trabajo se estudiaron los efectos de la relación de aspecto de la fibra de basalto (BFA), el contenido de fibra de basalto (BFC) y el contenido de fibra de polipropileno (PFC) en las propiedades mecánicas básicas del hormigón reforzado con fibra híbrida de basalto-polipropileno (BPHFRC) mediante un ensayo ortogonal. Además, se examinó el modo de fallo del hormigón mediante microscopio electrónico de barrido (SEM). Los resultados muestran que la mezcla de BF y PF conduce a un efecto híbrido positivo, y el impacto de BFC es el más significativo. Las resistencias a la compresión cúbica y axial disminuyen con el aumento del BFC. La combinación de A2B1C2 (BFA=800, BFC=0,2%, PFC=0,3%) aumentó las resistencias a la compresión cúbica y axial en un 13,73% y un 24,00%, respectivamente. La combinación de A2B2C3 (BFA=800, BFC=0,15%, PFC=0,2%) incrementó las resistencias a la tracción y a la flexión en un 32,40% y un 39,13%, respectivamente. Los modelos de predicción de la resistencia son fiables. El SEM observó que el puenteado de las fibras impedía el inicio y el crecimiento de las grietas.

PALABRAS CLAVE: Fibra de basalto; Fibra de polipropileno; Fibra híbrida; Propiedades mecánicas; Análisis microestructural.

1. INTRODUCTION

Concrete raw materials have numerous sources and economic value. Other building materials cannot shake the position of concrete in civil engineering construction (1, 2). However, concrete has some disadvantages in practical applications due to its low tensile strength (1/10-1/20 of the compressive strength (4)) and brittleness (5, 6). Effective improvement of concrete defects by fiber-modified PC is one of the breakthroughs in modern research on concrete structure technology (8). Fiber as a reinforcing material and other materials mixed with concrete are called fiber reinforced concrete (FRC) (7). FRC technology is easy to apply (9). Adding fibers into concrete can improve its mechanical properties, particularly the splitting tensile strength, flexural strength, and ductility performance. Furthermore, the incorporation of fibers in concrete results in reductions in the shrinkage and creep deformations of concrete. The construction section size of FRC is small, and the service life is prolonged (5). From natural fibers to artificial fibers, especially glass fiber, synthetic fiber, carbon fiber, and steel fiber can effectively improve the performance of concrete (10). Vahid reviewed the appropriate amount of fiber to improve the compressive strength. However, exceeding 2% fiber content reduces strength due to decreased working performance and increased porosity (11). Therefore, it is widely used in engineering practice. In 1982, the first composite highway bridge in the world was built in Mi Yun County, Beijing, with a span of 20.7 m, a width of 9.2 m, and a design load of about 80 tons (9).

Compared with steel, glass, and carbon fiber, BF is more resistant to weathering, high temperature (26), water, acid, and alkali damage (27). BF has numerous advantages, including a low price, energy-saving and environmental protection properties, high elastic modulus, good physical and mechanical characteristics, and excellent compatibility with concrete (21, 28, 29). Moreover, there is no risk of steel fiber reducing the durability of concrete, as mentioned in references (4, 12, 24, 25). It is a new material for strengthening concrete.

The performance of FRC depends on various factors, including the type of fibers, mixing method, number and size, geometry, orientation, and matrix properties (13-17). Khan M. discovered that when the BF content is 0.05%, the strength of the hybrid fiber reinforced concrete (HFRC) with different BFA outperformed that of FRC with a single-length fiber (22). Kabay added BF to concrete, significantly improving its flexural strength, fracture energy, and wear resistance but reducing its compressive strength (31). Algin et al. studied the workability and mechanical properties of self-compacting concrete enhanced with BF. The results showed that the flexural and splitting tensile strengths were the highest when the concrete was mixed with 24 mm and 0.5% BF, while the highest compressive strength was obtained when it was mixed with 12 mm and 0.1%, as well as 24 mm and 0.1% of BF (32). Lv et al. exhibited that the cubic compressive, splitting tensile, and flexural strengths of concrete initially increased and then decreased with the increase in the BFA. The appropriate content was within 0.15% (33). In previous studies, it has been observed that incorporating BF improved the fracture energy of concrete (31, 34, 35). Zhao et al. found that both the initial fracture toughness and unstable fracture toughness increased first and then decreased with the increase in fiber content. BF, with a length of 6 mm and a content of 0.2%, had the best toughening effect on concrete (4). The fracture performance is better with low short-fiber content than high long-fiber content (36).

PF has a low elastic modulus and low price. Its ductility is more excellent than that of BF, which is more conducive to the deformation performance of concrete, reducing plastic shrinkage and inhibiting crack propagation, thereby improving the mechanical properties and durability of concrete (19, 30). Zhu et al. utilized organic modified polypropylene fiber (OMPF) to enhance concrete's toughness, flexural strength, and seismic performance. OMPF has a lower specific gravity and better corrosion resistance than steel fiber (37). Luo et al. studied the optimum aspect ratio (L/D) of coarse PF is better than that of fine PF when the fixed content is constant (38). According to the results of He et al., adding fiber has no noticeable effect on compressive strength, but it significantly improves splitting tensile strength. In the case of high-content PF concrete, they can continue to bear the load even after the initial crack. The peak load and flexural strength increase initially with the increase in fiber content but then decrease (39). Ahmed et al. found that when the fiber content is less than 0.9%, the compressive strength and elastic modulus of FRC increase with the increase of PFC, which is helpful for microcrack arrest and has a more significant effect on flexural-tensile strength (18).

Depending on the size and type of fiber, a single fiber only works on one side. Cracking is a multi-level damage to concrete (19). Therefore, multi-size or multi-type fibers with reasonable hybrid ratios can give full play to their respective advantages, complement each other, and form a positive hybrid effect. Hybrid fibers with reasonable proportions work together with concrete to bridge at different levels and loading stages in the matrix to inhibit crack initiation and propagation and improve the multi-scale performance of concrete, such as ductility, crack resistance, energy absorption, and durability. The overall performance is more effective than a single fiber (13, 14, 19-22). Shi et al. investigated the mechanical properties of BPHFRC. They discovered that when the concrete contained 0.1% BF and 1% PF, it exhibited excellent flexural strength, strength after initial cracking and energy absorption performance. The fracture energy of concrete plays a significant role in determining the behavior of FRC after cracking (40). Huang et al. discovered that when the total amount of hybrid fiber is equal, the enhancement effect of BF on the splitting tensile strength of HFRC is more significant than that of PF. This is because BF has higher strength and stiffness than PF. BF carries most of the tensile stress during crack propagation, while PF breaks and provides auxiliary strengthening (41). It was reported by Fu et al. that the splitting tensile strength of concrete increases initially and then decreases with an increase in hybrid fiber content (0.1% to 0.2%). This strength is higher than that of a PC. The most significant strengthening effect is seen with 0.1% mixed fiber. Additionally, it was observed that the strengthening effect of BF is greater than that of PF (6). Combining fibers can improve flexural strength, toughness, and fracture energy more effectively than using a single fiber type (7).

The fracture energy of fiber absorption is also influenced by orientation. Brandt indicated that the optimum orientation angle of fibers with the orientation angle of fibers was the only variable, and the maximum fracture energy was the target (17). Mu et al. used a uniform magnetic field to influence the orientation arrangement of steel fibers in cement mortar to make ASFRC. The splitting tensile strength and flexural strength of ASFRC were more than 100% higher than SFRC (42). Failure caused by stress concentration near microscopic defects (5). Afroz et al. observed by SEM that the fiber in the concrete into a three-dimensional network, and the concrete components of the bond occlusion are better so that the microstructure is more compact, the concrete failure occurs when the fiber fracture, so basalt fiber reinforced concrete (BFRC) brittle failure (43). Jiang et al. found that the bonding between the BF and the concrete matrix interface was good in the early stage by SEM. However, after 28 days, debonding was observed between the substrate and the BF. Mercury intrusion porosimeter (MIP) detected higher porosity of the BFRC (25).

The analysis of these mechanical properties is a critical issue in the design of engineering structures. Therefore, a research program was proposed and carried out.

Currently, there is little research data on the hybrid of BF and PF. The research on BFRC has focused primarily on fiber content, with few studies conducted on fiber L/D. The quantitative relationship between the mechanical properties of BPHFRC and fiber content and L/D remains unclear. Therefore, this paper uses the orthogonal test method to design a three-factor and three-level orthogonal test group to study the influence of the BFA, BFC, and PFC on the cubic compressive, splitting tensile, axial compression, and flexural strengths indexes of BPHFRC, and to find the best content, to provide theoretical support for engineering applications. Additionally, the prediction models of concrete strength are established.

2. EXPERIMENTAL DESIGN

2.1. Test materials

Ordinary Portland cement (P.O 42.5) produced by the Sunnsy Group located in Huludao, China, was used in the present study. Table 1 shows the chemical composition of cement. The coarse aggregate is granite crushed stone with a particle size ranging from 5 mm to 20 mm. The fine aggregate is natural river sand with a fineness modulus of 2.47. The particle size distribution curve of fine and coarse aggregates is shown in Figure 1. The water used to mix the materials was drinkable tap water in Jinzhou. The BF characteristics are length 6/12/18 mm, diameter 0.015 mm, BFA=400/800/1200, density 2.85 g·cm^{-3}, tensile strength 3250 MPa, modulus of elasticity 100 GPa. The PF properties have the following parameters: length 12 mm, diameter 0.030 mm, density 0.92 g·cm^{-3}, tensile strength 550 MPa, and modulus of elasticity 3.95 GPa. Table 2 summarizes the main properties of BF and PF. The appearance morphology of the two fiber types is shown in Figure 2. Details of the mixture proportion of concrete are listed in Table 3. The mix design for cement: fine aggregate: coarse aggregate was 435 kg/m^3: 652 kg/m^3: 1028 kg/m^3 with a water/binder (W/B) ratio of 0.48. The polycarboxylate superplasticizer is 0.5% of the cement.

Table 1. Chemical composition of cement (wt%).

Composition	CaO	SiO_2	Al_2O_3	Fe_2O_3	MgO	Na_2O	SO_3	K_2O
Cement	61.60	22.40	5.07	4.25	1.58	0.33	2.35	1.1

Table 2. Physical and mechanical properties of the various fibers used.

Fiber Type	Diameter D/μm	Length L/mm	Aspect ratio (L/D)	Density /g·cm^{-3}	Elastic modulus /GPa	Tensile strength /MPa	Elongation /%
BF	15	6/12/18	400/800/1200	2.70	90-110	3000-3500	3.2
PF	30	12	400	0.92	3.95	550	40

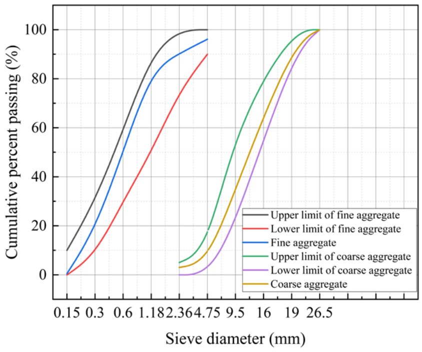

Figure 1. Particle size distribution curve of aggregates.

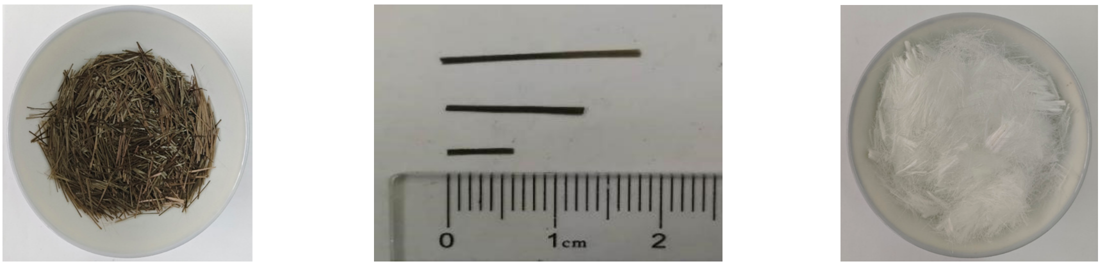

(a) (b) (c)

Figure 2. Appearance morphology of fiber. (a) Basalt fiber. (b) Basalt fiber length. (c) Polypropylene fiber.

Table 3. Mixture proportion of concrete.

Cement (kg/m^3)	Water (kg/m^3)	Fine aggregate (kg/m^3)	Coarse aggregate (kg/m^3)	W/B ratio
435	210	652	1028	0.48

2.2. Orthogonal experimental design

To study the influence of BFA (Factor A), BFC (Factor B), and PFC (Factor C) on the cubic compressive, splitting tensile, axial compressive, and flexural strengths of FRC, the orthogonal test scheme is selected, as shown in Table 4. There are three fiber aspect ratios (400, 800, and 1200) and three fiber content (0.1%, 0.2%, and 0.15%). Nine experiments were used to study the entire experimental parameters using the $L_9(3^4)$ orthogonal array for mechanical properties.

Table 4. Factors and levels of orthogonal design.

Factor ID	Factor description	Level 1	Level 2	Level 3
A	basalt fiber aspect ratio (BFA)	400	800	1200
B	basalt fiber content (BFC)	0.1	0.15	0.2
C	polypropylene fiber content (PFC)	0.1	0.15	0.2

2.3. Specimens fabrication

Before the test, the coarse and fine aggregate should be placed outdoors to dry to ensure drying. The material should be weighed strictly according to the test mix ratio, and the concrete mixer should be used for uniform mixing. Firstly, clean the pan mixer with a small quantity of water, then pour the coarse and fine aggregates and cementitious materials into the mixer and dry mixing for 60 seconds. Subsequently, BF and PF were manually dispersed and evenly mixed with the mixture for 60 seconds to avoid fiber agglomeration into balls. After that, water was added in batches and mixed for 3 minutes. Finally, the concrete mixture is cast in the test mold, which is coated with the mould release agent in advance, and the vibration is for 30 seconds to achieve a uniform distribution and density throughout the concrete. Due to the water absorption of fiber and the bonding effect between the fiber and the paste, the fluidity of fresh concrete decreases with the increase in the content of fiber. The vibration time of FRC should be longer than that of PC. After vibration, the mold is numbered, and the specimens are demoulded and cured after 24 hours.

The production and test methods conform to the Chinese Standard (GB/T 50081-2019) (44). Compressive and splitting tensile strengths were obtained using cubic specimens with a side length of 100 mm. In contrast, axial compressive and flexural strengths were obtained using prismatic specimens with a side length of 100×100×300 mm and 100×100×400 mm, respectively. Each mechanical property of each group produces three specimens and takes the arithmetic mean. The difference between the maximum, minimum, and intermediate values should not exceed 15% of the intermediate value. The span of the flexural experiment was 300 mm. The loading speed of cubic compressive and axial compressive strength is 0.5 MPa/s. In addition, the loading speed of split tensile and flexural strength is 0.05 Ma/s.

3. TEST RESULTS AND ANALYSIS

3.1. Test results

The results of the strength test for PC and BPHFRC are shown in Table 5 and Figure 3. We know that the cubic compressive strength, splitting tensile strength, axial compressive strength, and flexural strength of BPHFRC are greater than those of PC, which indicates that the incorporation of BF and PF into concrete is beneficial to improving its mechanical properties. Simultaneous visual analysis of the results of the nine groups of BPHFRC tests shows that groups A2B1C2 and A2B2C3 have the best performance in terms of mechanical properties. When the BFA is 800, the BFC is 0.1%, and the PFC is 0.15%. Moreover, the cubic and axial compressive strengths peak at 47.22 MPa and 37.21 MPa, respectively. The splitting tensile and flexural strengths peaked at 4.72 MPa and 6.43 MPa, respectively. When the BFA is 800, the BFC is 0. 15%, and the PFC is 0.20. Compared with PC, both strength increases of the A2B1C2 group are 13.73% and 23.54%, respectively, and both strength increases of the A2B2C3 group are 32.96% and 38.88%, respectively, indicating that the three factors have the most significant influence on the flexural strength of BPHFRC.

The mechanical properties of BPHFRC first increased and then decreased with the increase of BFA. When the optimum BFA was 800, the cubic and axial compressive strengths gradually decreased with the increase in fiber content. In contrast, the splitting tensile and flexural strengths increased and then decreased. It can be concluded that the appropriate amount of L/D ratio and fiber content can better optimize the mechanical properties of BPHFRC.

Table 5. Test results.

Specimen		PC	A1B1C1	A1B2C2	A1B3C3	A2B1C2	A2B2C3	A2B3C1	A3B1C3	A3B2C1	A3B3C2
Factor ID	A	-	400	400	400	800	800	800	1200	1200	1200
	B	-	0.10	0.15	0.20	0.10	0.15	0.20	0.10	0.15	0.20
	C	-	0.10	0.15	0.20	0.15	0.20	0.10	0.20	0.10	0.15
f_{cu}	$\bar{X}$	41.52	45.31	44.34	41.73	47.22	44.84	41.95	45.53	41.72	41.83
	σ	1.25	1.08	0.79	0.77	0.69	0.77	0.85	0.56	1.17	1.17
f_{ts}	$\bar{X}$	3.55	3.61	4.18	3.74	4.29	4.72	3.71	4.32	4.22	3.79
	σ	0.12	0.25	0.37	0.18	0.32	0.22	0.33	0.42	0.12	0.11
f_{ts}/f_{cu}	$\bar{X}$	0.086	0.080	0.094	0.090	0.091	0.105	0.088	0.095	0.101	0.091
	σ	0.005	0.004	0.01	0.003	0.007	0.006	0.006	0.011	0.004	0.005
f_c	$\bar{X}$	30.12	35.31	34.21	31.73	37.21	34.84	32.21	35.53	31.74	31.82
	σ	0.62	1.4	0.58	0.73	0.4	0.85	0.58	0.67	0.48	0.81
f_f	$\bar{X}$	4.63	5.32	6.15	5.52	5.83	6.43	5.42	5.62	5.73	5.34
	σ	0.28	0.6	0.19	0.56	0.45	0.22	0.54	0.53	0.24	0.2
f_f/f_{cu}	$\bar{X}$	0.112	0.117	0.139	0.132	0.123	0.143	0.129	0.123	0.137	0.128
	σ	0.01	0.011	0.005	0.015	0.008	0.003	0.017	0.011	0.003	0.008

Note: $\bar{X}$ (mean), σ (standard deviation), PC (Plain concrete), For example, A3B1C3 (BFA=1200, 0.1% BF, 0.2%.PF). f_{ts}/f_{cu} (Tension-Compression Ratio), f_f/f_{cu} (Flexural-Compression Ratio), f_{cu}、f_{ts}、f_c、f_f are BPHFRC cubic compressive strength, splitting tensile strength, axial compressive strength, flexural strength, MPa.

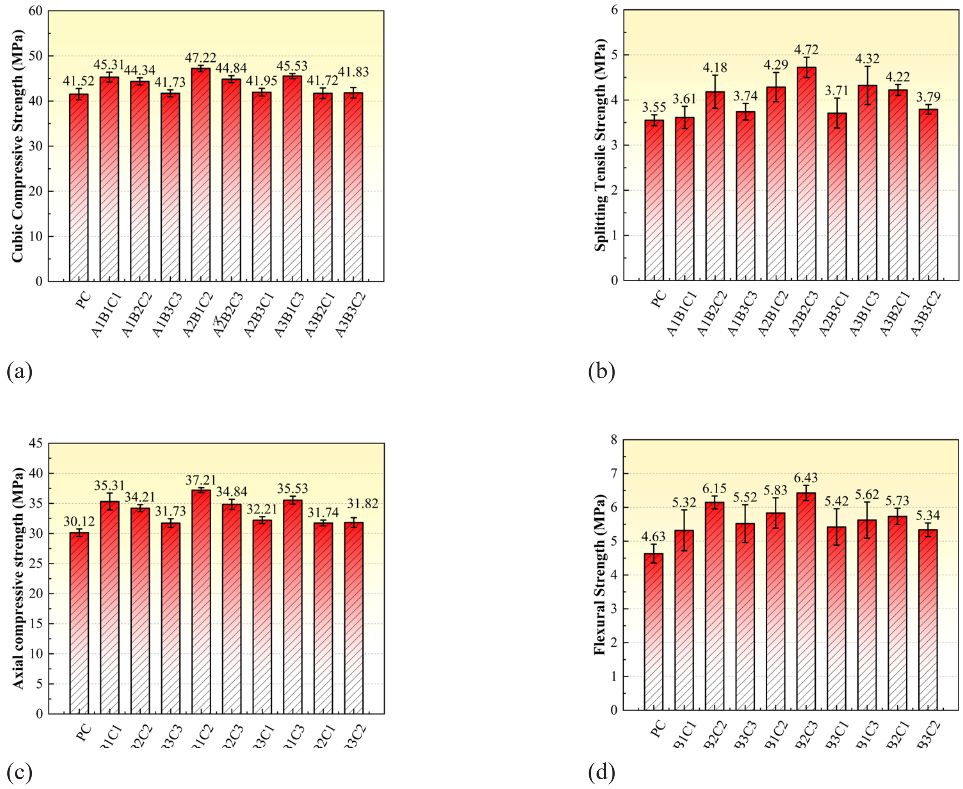

Figure 3. The mechanical properties of PC and BPHFRC. (a) Cubic compressive strength. (b) Splitting tensile strength. (c) Axial compressive strength. (d) Flexural strength.

3.2. Range analysis

The range analysis results of cubic compressive strength, splitting tensile strength, axial compressive strength, and flexural strength of BPHFRC in Table 5 are shown in Table 6. The influence trend of three factors on cubic compression strength, splitting tensile strength, axial compressive strength, and flexural strength of BPHFRC is drawn, as shown in Figure 4 (a) - (d). The average 1, average 2, and average 3 in Table 6 represent the average strength of each factor at three levels, respectively, to obtain the order of primary and secondary factors, the optimal level combination, and the changing trend of strength of each factor at different levels. The range R represents the influence of each factor on the index. The factor index effect curve is shown in Figure 4.

Table 6. BPHFRC strength range analysis table.

	f_{cu}			f_{ts}			f_c			f_f		
Factor	(A)	(B)	(C)	(A)	(B)	(C)	(A)	(B)	(C)	(A)	(B)	(C)
Average 1	43.79	46.02	42.99	3.84	4.07	3.85	33.75	36.02	33.09	5.66	5.59	5.49
σ	0.21	1.02	0.1	0.22	0.18	0.08	0.54	0.4	0.35	0.24	0.37	0.08
Average 2	44.67	43.63	44.46	4.24	4.37	4.09	34.75	33.6	34.41	5.89	6.10	5.77
σ	0.51	1	0.32	0.22	0.12	0.02	0.51	0.4	0.4	0.37	0.18	0.14
Average 3	43.03	41.84	44.03	4.11	3.75	4.26	33.03	31.92	34.03	5.56	5.43	5.86
σ	0.84	2.08	0.39	0.21	0.11	0.11	0.2	0.14	0.32	0.16	0.35	0.23
Range R	1.64	4.18	1.47	0.40	0.63	0.41	1.72	4.10	1.33	0.33	0.68	0.37
Secondary factors		B > A > C			B > C > A			B > A > C			B > C > A	
Best level	A2	B1	C2	A2	B2	C3	A2	B1	C2	A2	B2	C3
Best level combination		A2B1C2			A2B2C3			A2B1C2			A2B2C3	

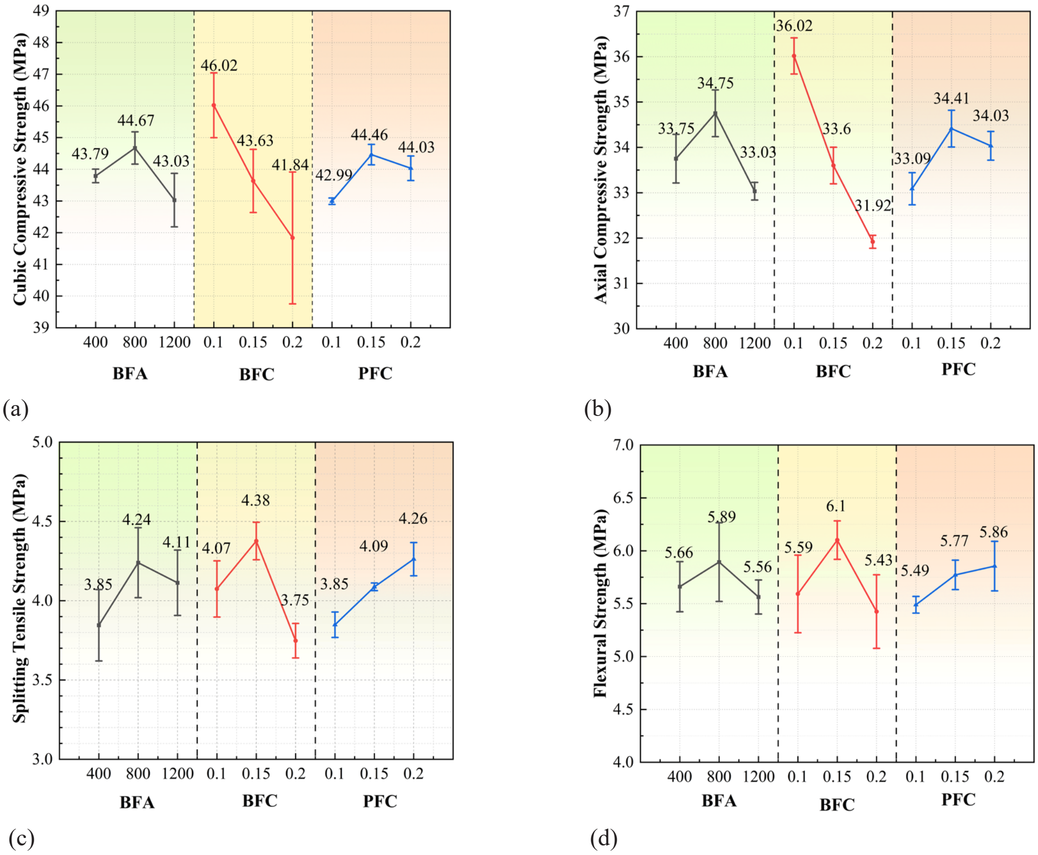

Figure 4. Variation trend of mechanical properties of BPHFRC. (a) Cubic compressive strength. (b) Axial compressive strength. (c) Splitting tensile strength. (d) Flexural strength.

It can be seen from Figure 4 (a) and Table 6 that the cubic compressive strength of orthogonal BPHFRC is higher than that of PC, showing a positive hybrid effect. In the orthogonal group, A2B1C2 has a maximum cubic compressive strength of 47.22 MPa, 13.73% higher than PC. A3B2C1 has a minimum cubic compressive strength of 41.72 MPa, 0.48% higher than PC. The cubic compressive strength increases and then decreases with the increase of BFA, with 800 as the optimum level. The BFA is from 400 to 800, and the cubic compressive strength increases by 2.01%. While the BFA is from 800 to 1200, the compressive strength decreased by 3.81%. The optimum BFA ranges from 400 to 800. The cubic compressive strength decreases with increased BFC, and 0.1% is the best level. From 0.1% to 0.2%, the cubic compressive strength reduces by 9.99%. Table 6 shows that BFC significantly affects cubic compressive strength. The cubic compressive strength increases and then decreases with the increase of PFC, and 0.15% is the optimum level. The cubic compressive strength increased linearly from 0.1% to 0.15% PFC, and the compressive strength at 0.2% PFC was slightly lower than that at 0.15% by 0.98%. The optimum content range was 0.1% to 0.15%. The order of factors affecting the cubic compressive strength of BPHFRC is B > A > C. The higher the cubic compressive strength value, the better. Therefore, the optimal level of the three factors is BFA of 800, BFC of 0.1%, and PFC of 0.15%, respectively. The optimal level combination is A2B1C2 and the worst is A3B3C1.

From Figure 4 (b) and Table 6, it can be seen that the splitting strength of orthogonal BPHFRC is higher than that of PC, showing a positive hybrid effect. The minimum splitting tensile strength of A1B1C1 in the orthotropic group is 3.61 MPa, which is 1.69% higher than that of PC. The maximum splitting tensile strength of A2B2C3 is 4.72 MPa, 32.96% higher than PC. The splitting tensile strength increases and decreases with increasing BFA, with 800 as the optimum level. The splitting strength increased by 10.42% from 400 to 800 and decreased by 3.16% from 800 to 1200. The optimal BFA range is 400 to 800. The splitting tensile strength increases and decreases with increasing BFC, with 0.15% being the optimum level. BFC, from 0.1% to 0.15%, increased the strength by 6.86%, while from 0.15% to 0.2%, decreased the strength by 16.53%. The optimum content range was 0.1% to 0.15%. The splitting tensile strength increased with increasing PFC, with 0.2% being the optimum level. The two levels of

0.15% and 0.2% increased the splitting tensile strength by 5.71% and 10.65%, respectively, compared to the 0.1% level. The optimal content ranges from 0.15% to 0.2%. It can be seen from Table 6 and Figure 4 (b) that the order of factors affecting the splitting tensile strength of BPHFRC is B > C > A. The higher the splitting tensile value, the better. Therefore, the optimal levels of the three factors are BFA of 800, BFC of 0.15%, and PFC of 0.2%. The optimal level combination is A2B2C3 and the worst is A1B3C1.

Figure 4 (c) and Table 6 indicate higher axial compressive strength of orthogonal BPHFRC than that of PC, demonstrating a positive hybrid effect. The maximum axial compressive strength of A2B1C2 is 37.21 MPa, 23.54% higher than PC. The minimum axial compressive strength of A1B3C3 is 31.73 MPa, 5.35% higher than PC. Axial compressive strength increases and decreases with increasing BFA, with 800 as the optimum level. From 400 to 800, the axial compressive strength increased by 2.97%. From 800 to 1200, the axial compressive strength decreased by 5.21%. The optimal BFA range is 400 to 800. The axial compressive strength decreases with the increase of BFC, and 0.1% is the best level. From 0.1% to 0.2%, the axial compressive strength reduces by 12.84%. The effect of BFC on axial compressive strength is significant, as shown in Table 6. The axial compressive strength increases and then decreases with the increase of PFC, with 0.15% being the optimum level. PFC, from 0.1% to 0.15%, increased the axial compressive strength by 3.99%, while from 0.15% to 0.2%, slightly decreased the axial compressive strength by 1.12%. The optimum content range was 0.1% to 0.15%. It can be seen from Table 6 and Figure 4 (c) that the factors affecting the axial compressive strength of BPHFRC are in the order of B > A > C. The higher the axial compressive strength value, the better. Therefore, the optimal levels of the three factors are BFA of 800, BFC of 0.1%, and PFC of 0.15%. The optimal level combination is A2B1C2, and the worst level is A3B3C1.

Figure 4 (d) and Table 6 show that the flexural strength of orthogonal BPHFRC is higher than that of PC, showing a positive hybrid effect. The flexural strength of A1B1C1 in the orthogonal group is 5.32 MPa, which is 14.9% higher than that of PC. The maximum flexural strength of A2B2C3 is 6.43 MPa, 38.88% higher than PC. The flexural strength increases and decreases with increasing BFA, with 800 being the optimum level. Flexural strength increased by 4.06% from 400 to 800 and decreased by 5.94% from 800 to 1200. The optimal BFA range is 400 to 800. The flexural strength increases first and then decreases with the increase of BFC, and 0.15% is the optimal level. BFC increased from 0.1% to 0.15%, and the strength increased by 9.12%, while from 0.15% to 0.2%, the strength decreased by 12.34%. The optimum content range is 0.1% to 0.15%. Table 4 shows that BFC has a significant effect on flexural strength. The flexural strength increases with the increase of PFC, and 0.2% is the best level. The two levels of PFC, 0.15% and 0.2%, increased the overall flexural strength by 5.10% and 6.74%, respectively, compared to the 0.1% level of PFC. The optimum content range is 0.15% to 0.2%. It can be seen from Table 6 and Figure 4 (d) that the order of factors affecting the flexural strength of orthogonal BPHFRC is B > C > A. The higher the flexural strength value, the better. Therefore, the optimal levels of the three factors are BFA of 800, BFC of 0.15%, and PFC of 0.2%. The optimal level combination is A2B2C3, and the worst level is A1B3C1.

3.3. Analysis of variance

The results of variance analysis of cubic compressive strength, splitting tensile strength, axial compressive strength, and flexural strength of BPHFRC are shown in Table 7. It can be seen from Table 7 that the influence of various factors on the cubic and axial compressive strengths of BPHFRC is B > A > C, which is consistent with the results of range analysis. The effect is that the BFC significantly affects the cubic and axial compressive strengths, and BFA and PFC have some effect on cubic and axial compressive strengths. The influence of various factors on the splitting tensile and flexural strengths of BPHFRC is B > C > A, which is consistent with the results of the range analysis. The effect of BFC on the splitting tensile and flexural strengths is particularly significant, and the impact of BFA and PFC on the splitting tensile and flexural strengths is substantial.

3.4. Tension-compression ratio and flexural-compression ratio

3.4.1. Tension-compression ratio

Table 5 and Figure 5 show that when the orthogonal combination is A2B2C3, the tensile-compression ratio achieves a maximum value of 0.105, which is 22.22% higher than that of PC. At this time, the BFA is 800, and the BFC and PFC are 0.15% and 0.2%, respectively. The tensile strength and tension-compression ratio are the largest at the same time. This shows that BF and PF play an excellent synergistic effect in the concrete matrix, and the enhancement of tensile performance is more significant than compressive performance. With the increase of hybrid fiber content, the tension-compression ratio decreases gradually.

Table 7. BPHFRC variance analysis table.

Test indicators	Factors	Square of deviance	Degree of freedom	Variance	F-ratio	F Critical value	Significance
Cubic compressive strength	A	4.057	2	2.028	11.916	F0.01 (2,2) = 99	(*)
	B	26.424	2	13.212	77.612	F0.05 (2,2) = 19	*
	C	3.427	2	1.714	10.067	F0.1 (2,2) = 9	(*)
	Error	0.340	2	0.170			
	Summation	34.249	8				
Splitting tensile strength	A	0.245	2	0.123	83.015	F0.01 (2,2) = 99	*
	B	0.589	2	0.295	199.429	F0.05 (2,2) = 19	**
	C	0.258	2	0.129	87.459	F0.1 (2,2) = 9	*
	Error	0.003	2	0.001			
	Summation	1.096	8				
Axial compressive strength	A	4.495	2	2.247	12.344	F0.01 (2,2) = 99	(*)
	B	25.450	2	12.725	69.889	F0.05 (2,2) = 19	*
	C	2.801	2	1.400	7.691	F0.1 (2,2) = 9	-
	Error	0.364	2	0.182			
	Summation	33.110	8				
Flexural strength	A	0.172	2	0.086	69.649	F0.01 (2,2) = 99	*
	B	0.748	2	0.374	303.270	F0.05 (2,2) = 19	**
	C	0.222	2	0.111	89.865	F0.1 (2,2) = 9	*
	Error	0.002	2	0.001			
	Summation	1.144	8				

Note: Significant means, ** means particularly significant, * means significant, (*) means some shadow, -means little effect.

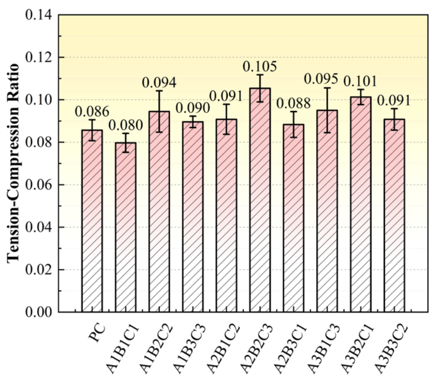

Figure 5. Tension-compression ratio of different fiber content.

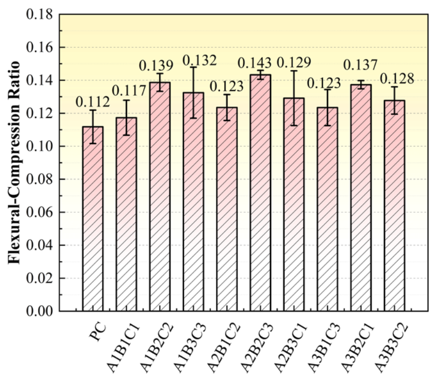

Figure 6. Flexural-compression ratio of different fiber content.

3.4.2. Flexural-compression ratio

Table 5 and Figure 6 show that when the orthogonal combination is A2B2C3, the maximum flexural-compression ratio is 0.143, 27.68% higher than that of PC. At this time, the BFA is 800, and the BFC and PFC are 0.15% and 0.2%, respectively. The flexural strength and flexural-compression ratio reach the maximum value simultaneously, and the toughness of the concrete reaches the best state. The flexural-compressive ratio of concrete mixed with two kinds of fibers increases significantly, indicating that hybrid fibers are the key factor in improving the flexural strength and toughness of the concrete.

3.5. Efficacy coefficient analysis

According to the range analysis and variance analysis, the influence of three factors on the strength of BPHFRC is inconsistent, and it is difficult to determine the optimal level combination. Therefore, the efficacy coefficient method is introduced to analyze the cubic compressive strength, splitting tensile strength, axial compressive strength, and flexural strength (41). The results are shown in Table 8. The maximum of specimen A2B1C2 is 371.97. Therefore, the optimal combination of cubic compressive strength, splitting tensile strength, axial compressive strength, and flexural strength is A2B1C2 (BFA of 800, BFC of 0.1%, and PFC of 0.15%.

Table 8. Results of efficacy factor value calculation.

Specimen	Index of strength				Efficacy coefficient				Total efficacy coefficient $\sum d_i$
	f_{cu}	f_{ts}	f_c	f_f	f_{cu} d_1	f_{ts} d_2	f_c d_3	f_f d_4	
PC	41.52	3.55	30.12	4.63	60.00	60.00	60.00	60.00	240.00
A1B1C1	45.31	3.61	35.31	5.32	86.6	62.05	89.28	75.33	313.26
A1B2C2	44.34	4.18	34.21	6.15	79.79	81.54	83.07	93.78	338.18
A1B3C3	41.73	3.74	31.73	5.52	61.47	66.5	69.08	79.78	276.83
A2B1C2	47.22	4.29	37.21	5.83	100	85.3	100	86.67	371.97
A2B2C3	44.84	4.72	34.84	6.43	83.3	100	86.63	100	369.93
A2B3C1	41.95	3.71	32.21	5.42	63.02	65.47	71.79	77.56	277.83
A3B1C3	45.53	4.32	35.53	5.62	88.14	86.32	90.52	82	346.99
A3B2C1	41.72	4.22	31.74	5.73	61.4	82.91	69.14	84.44	297.89
A3B3C2	41.83	3.79	31.82	5.34	62.18	68.21	69.59	75.78	275.75

3.6. BPHFRC strength prediction model

According to the theory of composite material mechanics, it is assumed that the strength of BPHFRC is composed of concrete matrix strength, BF reinforcement, and PF reinforcement. Assuming that the strength regression model is (46):

$$f = \beta_1 + \beta_2 \times x_2 + \beta_3 \times x_3 + \beta_4 \times x_2^2 + \beta_5 \times x_3^2 + \beta_6 \times x_1 \times x_2 + \beta_7 \times x_2 \times x_3 \quad [1]$$

In the formula: f is concrete cubic compressive strength, axial compressive strength, splitting tensile strength, flexural strength, MPa; β_1, β_2, β_3, β_4, β_5, β_6, β_7 are regression coefficients; x_1 is the aspect ratio of BF; x_2 is the content of BF, %; x_3 is the content of PF, %.

SPSS software was used to perform multivariate nonlinear statistical analysis. Regression analyses of cubic compressive strength, axial compressive strength, splitting tensile strength, and flexural strength were performed to derive the value of each regression coefficient and the coefficient of determination R^2.

Table 9. Fitting parameters and coefficient of determination values.

Model	β_1	β_2	β_3	β_4	β_5	β_6	β_7	R^2
f_{cu}	38.33	-41.473	161.982	118	-416.45	-189.8	-0.009	0.873
f_{ts}	-1.235	58.667	14.225	-185.333	-8.5	-48.667	0.001	0.879
f_c	29.135	-45.293	154.001	148.667	-378.55	-218.866	-0.009	0.857
f_f	-1.527	78.087	24.319	-238	-46.65	-46.6	-0.002	0.856

Table 10. The relative error between predicted value and experimental value (%).

Model	1	2	3	4	5	6	7	8	9
f_{cu}	0.38	-1.22	-1.08	1.05	2.48	0.95	-1.53	1.46	0.003
f_{ts}	-1.64	-2.93	0.44	5.11	3.39	2.72	-2.55	0.89	-0.46
f_c	0.43	-1.74	-1.5	1.45	3.28	1.21	-2.15	-2.07	-0.19
f_f	-0.02	-1.8	-0.44	3.24	3.72	2.51	-1.91	-0.13	00.92

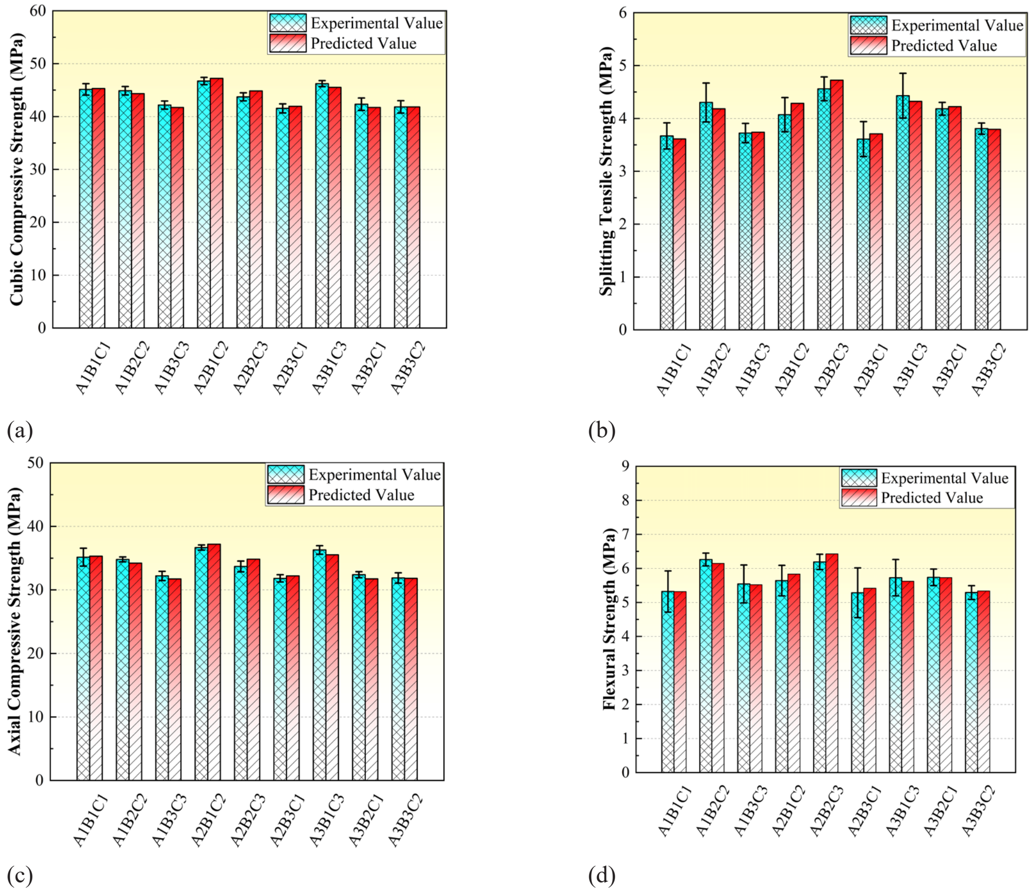

FIGURE 7. The relative error between the predicted value and experimental value. (a) Cubic compressive strength. (b) Splitting tensile strength. (c) Axial compressive strength. (d) Flexural strength.

From Table 9, the determination coefficient of the model is more significant than 0.98, indicating that the strength model is reliable. According to Table 10 and Figure 7, the relative error of the prediction model for cubic and axial compressive and flexural strengths are within 3.72%, while splitting tensile strength is under 5.11%. The strength model has high accuracy, which can provide a reference for optimizing the mix ratio of laboratory FRC and practical engineering.

3.7. Microstructure analysis

Macroscopic concrete is regarded as having two phases: aggregate and cement paste. There is also a weak interfacial transition zone (ITZ) between the two microscopic phases, which significantly influences the mechanical properties of concrete (47). This paper used the German ZEISS Sigma 300 scanning electron microscope (SEM) to analyze the concrete failure specimens cured for 28 days.

3.7.1. The failure morphologies of the concrete specimens

Figure 8 and Figure 10 are the fractured morphologies of PC and BPHFRC. Different from the vertical cracks of PC, the cracks at the fracture surface of BPHFRC were deflected due to the bridging effect of the fibers that changed the direction of the cracks. In addition, the air carried by the fibers, the porosity of BPHFRC, is also higher than that of PC (48). As shown in Figure 10, the fibers are disorderly distributed in the concrete to form a three-dimensional network structure, which is used as the attachment point of the cement paste to make it more widely distributed.

It can be seen from Figure 10 (a) that a large part of the BF is still wrapped in the concrete when BPHFRC is damaged, and more cement hydration products are attached to the surface of the exposed part, indicating that the bonding performance between the BFs and the concrete matrix is good. Hydrophilic BFs absorb water to promote the hydration of surface cementitious materials (5,49), resulting in good bonding properties with the concrete matrix. As can be seen from Figure 12 (d), when the concrete mixed with PF is damaged, the PFs have a large pull out length, and its surface is relatively smooth, which indicates that the bonding performance between the PFs and the concrete matrix is poor. The deformation of PF after failure indicates that PF plays a ductile role. Compared with basalt fiber, it can provide higher deformation ability and better fracture energy (50), increasing the deformation performance of concrete. PFs are hydrophobic fibers (51), so there is a gap between PFs and cement paste, indicating no chemical reaction between the two, increasing the weak interface layer, as shown in Figure 11. The synergistic effect of the BFs and PFs was beneficial for improving the strength and deformation properties of the concrete (5).

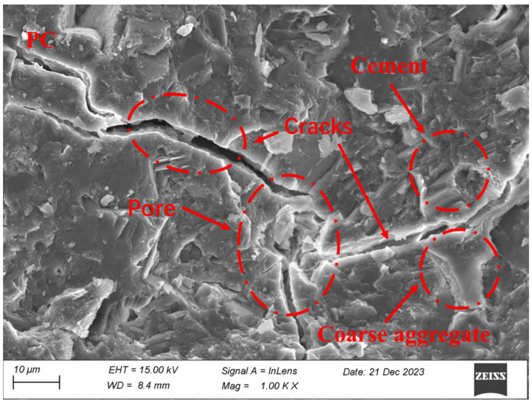

FIGURE 8. SEM micrograph of PC. Microscopic Cracks and pores.

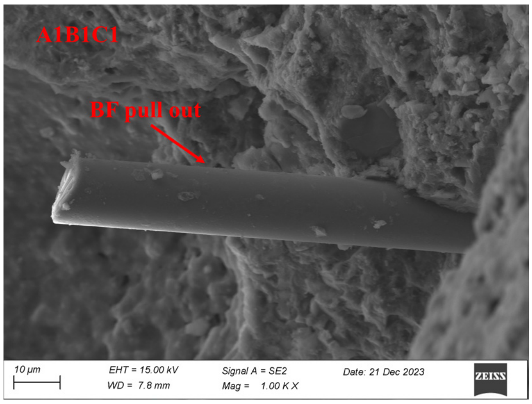

FIGURE 9. SEM micrograph of A1B1C1. BF pull out.

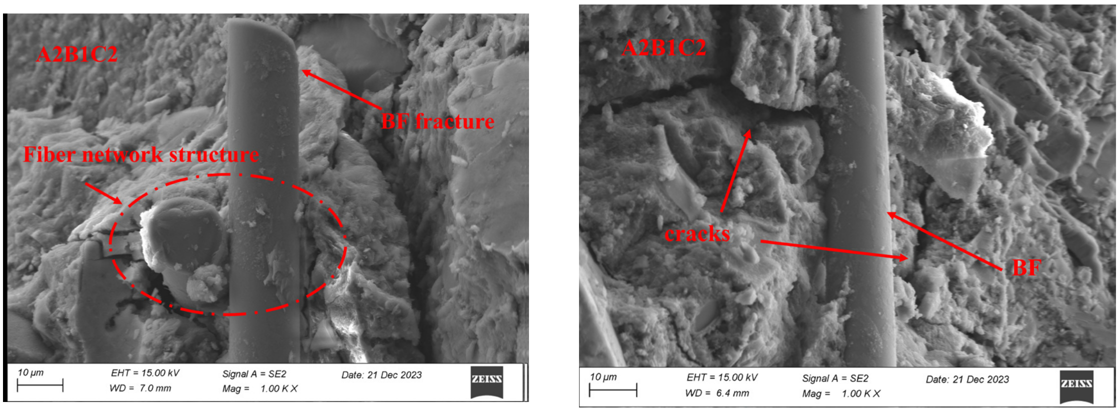

(a) (b)

FIGURE 10. SEM micrograph of A2B1C2. (a) Fiber three-dimensional network structure and fracture. (b) BF oriented vertical cracks and cracks deflection.

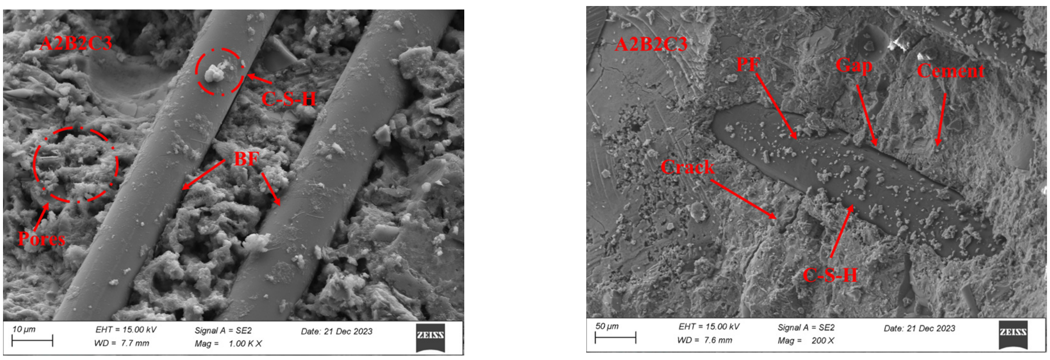

(a) (b)

FIGURE 11. SEM micrograph of A2B2C3. (a) More fiber content and more pores. (b) Gap between polypropylene and cement.

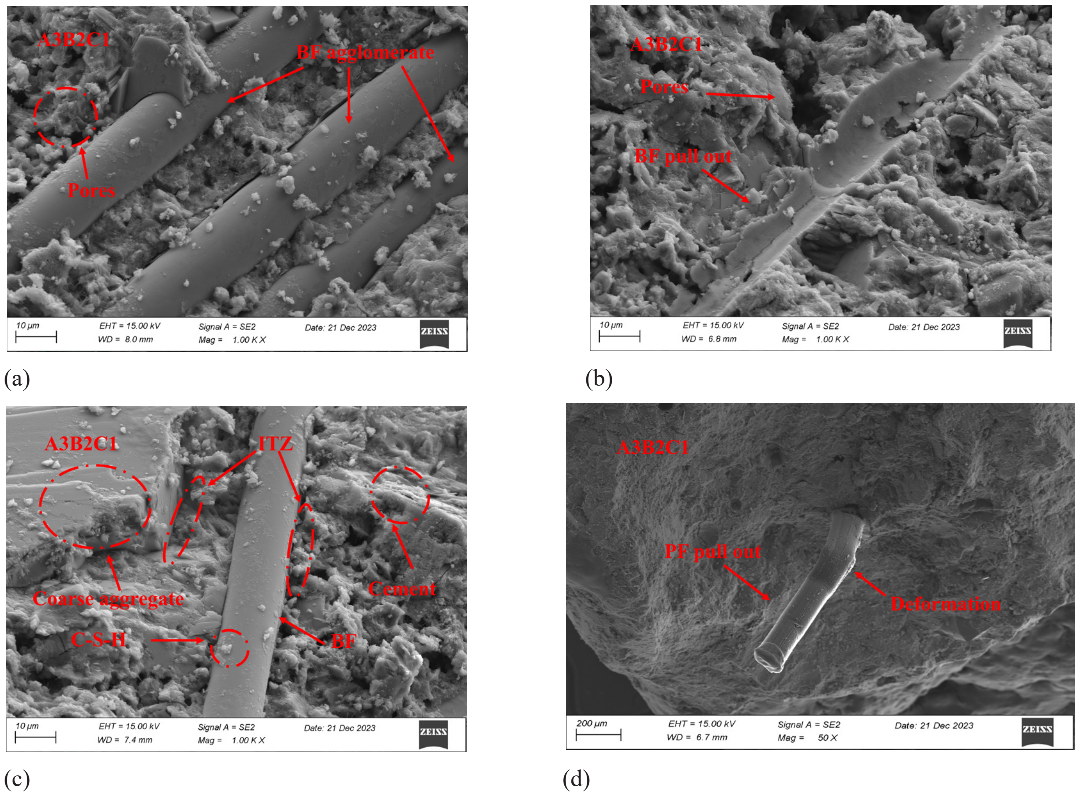

Figure 12. SEM micrograph of A3B2C1. (a) Fiber agglomeration. (b) Lack of adhesion pull out. (c) Interface between fiber and cement matrix. (d) PF pull out and deformation.

It can be observed from Figs. 8, 9, 10, and 11 that the dispersion of BFA of 400 (6 mm) is better than that of BFA of 800 and 1200 (12 mm and 18 mm) (52). However, A1B1C1 has low mechanical properties, especially the splitting tensile and flexural strengths, because the bond strength of the BFA of 400 is not enough to be pulled out, and the content of the BF and PF is small (0.1% BF, 0.1% PF), as shown in Figure 9. When the BFC is 0.10%, the BF cannot form a load-bearing skeleton in the BPHFRC (53).

The BF in A3B2C1 with an L/D ratio of 1200 is too long and has a large content (0.15% BF). The content of PF is less (0.1% PF). The interfacial transition zone increases, and the structure becomes looser. BF and PF are easy to agglomeration and involved in the air, reducing the degree of compactness. The reason may be that a larger L/D ratio causes the fibers to tend to agglomeration (52). Cement paste cannot wrap around agglomerated fibers well, resulting in reduced fiber-matrix interphase bond strength and fibers being pulled out. The fibers are distributed along the coarse aggregate and parallel to the micro-cracks at the interface between coarse aggregate and cement paste. The wall effect reduces the fiber reinforcement effect.

Figure 10 shows that the BFA of 800 fractures is more than that of those with an L/D ratio of 400, and the BF fracture has a smooth fracture surface. The explanation could be that a larger L/D ratio of fibers shows a more apparent bridging effect and stronger pulling out resistance, which helps it bear the load along with the concrete (54). Compared to the BFA of 1200, a moderate content of BF with an L/D ratio of 800 intersects microcracks at the coarse aggregate and mortar interface, preventing cracks development. Figures 10 and 12 show that the 800 BFA has a better orientation than the 1200 BFA, with more fibers passing through the cracks, forming a network structure and better bridging angle. Consequently, the transverse deformation of concrete is restricted, thereby enhancing the macroscopic mechanical properties.

This results in the damage changing from brittle to plastic, making it a more reinforced material (55). Therefore, A2B1C2 and A2B2C3 have better mechanical properties. It was observed that BF with an appropriate content of 800 in the L/D ratio was uniformly distributed and showed a positive hybrid effect. A2B1C2 has more cracks than A2B2C3, as in Figures 10, 11. A2B2C3 has a higher fiber content (0.15% BF, 0.20% PF), which can reduce the initial cracks and prevent the development of cracks, thus effectively improving the splitting tensile and flexural strengths. However, the total porosity increases with the increase of fiber content, which reduces the compactness of concrete, thus reducing the cubic compressive and axial compressive strengths. So, the cubic and axial compressive strengths of A2B1C2 are the best.

The micro-morphology varies with fiber content and L/D. As shown in Figure 5, the various mechanical properties of FRC are improved compared to PC. For cubic compressive and axial compressive strengths, A2B1C2 is the best, and A3B2C1 is the worst. And for splitting tensile and flexural strength, A2B2C3 is optimal, and A1B1C1 is the worst.

3.7.2. Hydration products

Portland cement is mainly composed of four clinker phases, alite (C_3S, Ca_3SiO_5), belite (C_2S, Ca_2SiO_4), tricalcium aluminate (C_3A, $Ca_3Al_2O_6$), and tetracalcium aluminoferrite (C_4AF, $Ca_4Al_2Fe_2O_{10}$), as well as a small amount of dihydrate gypsum ($CaSO_4 \cdot 2H_2O$) and limestone ($CaCO_3$). After hydration reaction, C_3S and C_2S form gel-like calcium-silicate-hydrate (C-S-H) and flake portlandite (CH, $Ca(OH)_2$), while C_3A and C_4AF react with gypsum to form ettringite (AFt, $3CaO \cdot Al_2O_3 \cdot 3CaSO_4 \cdot 32H_2O$) and monosulfoaluminate (AFm, $3CaO \cdot Al_2O_3 \cdot CaCO_3 \cdot 12H_2O$). As shown in Table 11.

Table 11. Hydration reaction.

Code	Hydration process	
C_2S	$2(2CaO \cdot SiO_2) + 4H_2O = 3CaO \cdot 2SiO_2 \cdot 3H_2O + Ca(OH)_2$	[2]
C_3S	$2(3CaO \cdot SiO_2) + 6H_2O = 3CaO \cdot 2SiO_2 \cdot 3H_2O + 3Ca(OH)_2$	[3]
C_3A	$3CaO \cdot Al_2O_3 + 6H_2O = 3CaO \cdot Al_2O_3 \cdot 6H_2O$	[4]
C_4AF	$4CaO \cdot Al_2O_3 \cdot Fe_2O_3 + 7H_2O = 3CaO \cdot Al_2O_3 \cdot 6H_2O + CaO \cdot Fe_2O_3 \cdot H_2O$	[5]
gypsum	$3CaO \cdot Al_2O_3 \cdot 6H_2O+3(CaSO_4 \cdot 2H_2O) + 19H_2O = 3CaO \cdot Al_2O_3 \cdot 3CaSO_4 \cdot 32H_2O$	[6]
	$3CaO \cdot Al_2O_3 \cdot 3CaSO_4 \cdot 32H_2O + 2(3CaO \cdot Al_2O_3 \cdot 6H_2O) = 3(3CaO \cdot Al2O_3 \cdot CaCO_3 \cdot 12H_2O)$	[7]

These compounds manifest as distinct crystal structures: hexagonal shapes indicate CH gel, flower-shaped structures signify C-S-H gel and needle-like formations represent AFt. As shown in Figure 13. There are AFt in cracks and pores, fibrous C-S-H gel and flake CH deposited in C-S-H gel, which is not easy to identify (56). The C-S-H gel wraps the unhydrated cement particles to form a network structure.

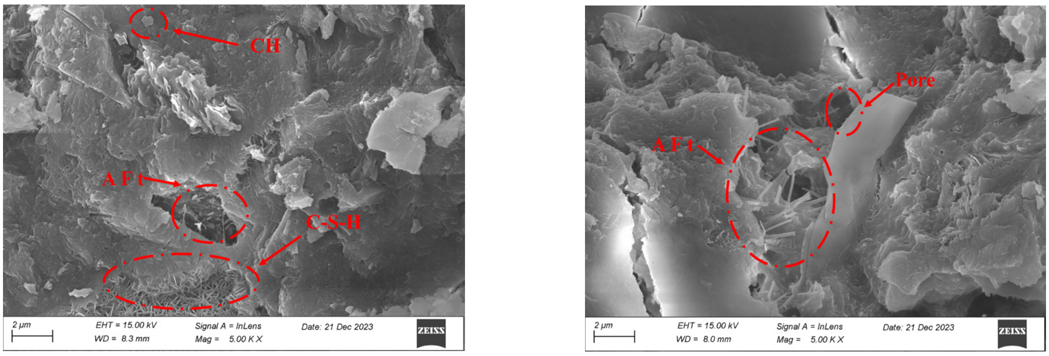

(a) (b)

Figure 13. SEM micrograph of hydration products.

The specific phase can be identified by its typical micro-morphology and information measured by EDS. The atomic ratio is usually used to determine the hydration products (57). The Ca/Si atomic ratio is one of the essential parameters to describe the C-S-H. Taylor (58) proposed an EDS point analysis of hydration products. When Ca/Si < 2.5, a large amount of C-S-H is generated, but the Ca/Si ratio increases, the content of C-S-H decreases, and the CH, AFt, and AFm content is relatively high. CH is the main hydration product when Ca/Si > 10 and (Al + Fe)/Ca and S/Ca < 0.04. CH is a crucial component in maintaining the alkalinity of cement. When (Al + Fe)/Ca > 0.4 and S/Ca > 0.25, AFm is considered the main hydration product. The Ca/Si atomic ratio can indirectly reflect the cement hydration products in the ITZ (59).

Figure 14 (A) shows that Ca/Si = 12.63, (Al + Fe)/Ca = 0.044, and S/Ca = 0.013. The main hydration product is CH, including C-S-H, AFt, and AFm. Figure 14 (B) shows that Ca/Si = 2.07. The main hydration products are C-S-H or calcium aluminosilicate hydrate (C-A-S-H), and there are also fewer CH, AFm, and AFt. C-S-H has good properties when the Ca/Si ratio is low.

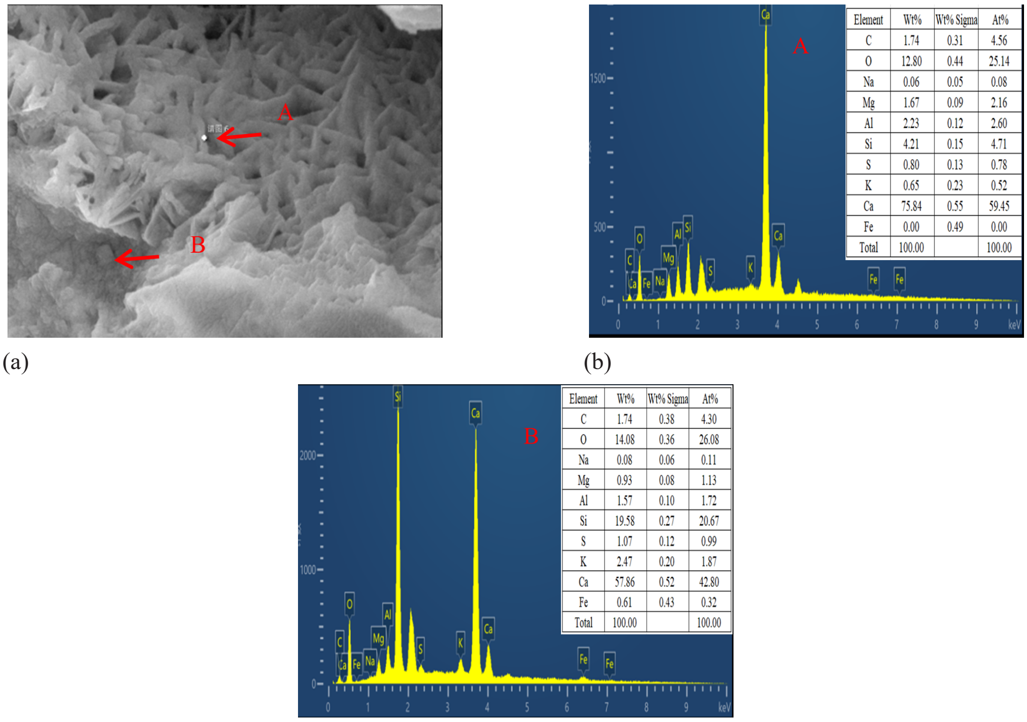

(a) (b)

(c)

Figure 14. (a) SEM micrograph. (b) EDS point-scan of A. (c) EDS point-scan of B.

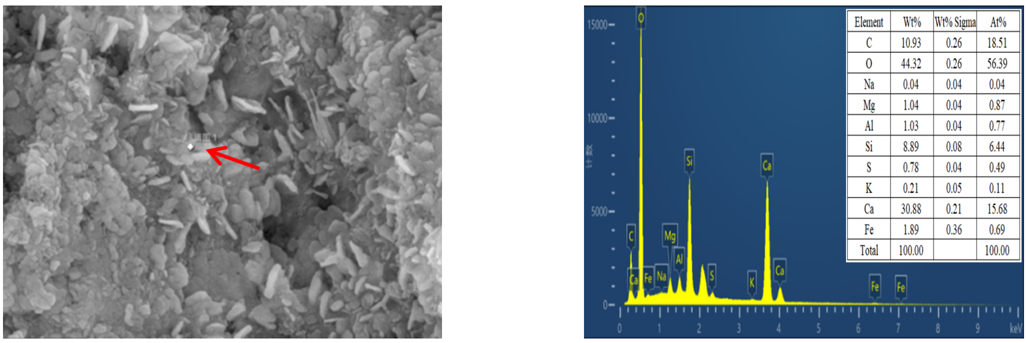

(a) (b)

Figure 15. (a) SEM micrograph. (b) EDS point-scan.

The selected point in Figure 15 contains three elements of C, O, and Ca. The atomic number of the O element is three times that of the Ca element, which may be $CaCO_3$. Ca/Si = 2.43. It also contains more C-S-H and a small amount of CH, AFt, and AFm.

The sample points in Figure 16 mainly include Ca, S, O, Al, and other elements. (Al + Fe)/Ca = 0.91 indicates that the main hydration products are AFt and AFm. The higher content of Mg element may be magnesia in cement. Periclase (free-state magnesia crystal) hydrates to form magnesium hydroxide, and the volume expansion is 118%, causing concrete damage (60). Undecomposed C-S-H reacts with Mg^{2+} to form magnesium silicate hydrate (M-S-H), accelerating the decrease of C-S-H content (61).

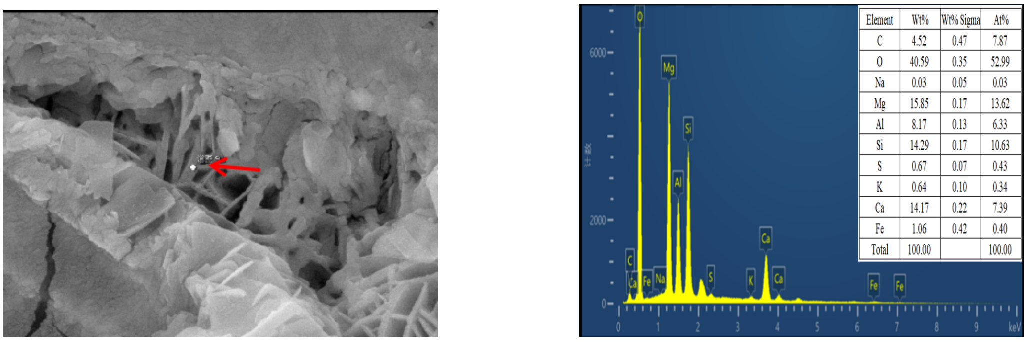

(a) (b)

FIGURE 16. (a) SEM micrograph. (b) EDS point-scan.

3.7.3. Interfacial transition zone

The ITZ is weak, and the density of the C-S-H gel is lower than that of other regions. However, many C-S-H gels still form a dense flocculation structure and contain amorphous porous materials (56).

Figure 8 shows the morphology of the crack at the interface between the cement paste and the aggregate. Where hydration products do not cover PC, the cracks are more significant. On the contrary, the crack of fiber reinforced concrete is not apparent, and the boundary separation between cement paste and aggregate is large (55).

Due to the hydrophobicity of PF, the interfacial adhesion between PF and C-S-H is mainly caused by the non-bonded interaction of PF and paste. At the same time, the chemical bond contributes less (62). Many hydroxyl groups (-OH) are attached to the surface of BF, which is hydrophilic. Hydroxyl groups react with water to form hydrogen-bonded. Liquids with intermolecular hydrogen-bonded are viscous. The hydration products connect the fibers into clusters, improve their tensile strength, and enhance the connection between fibers and concrete (63).

It is generally believed that the performance of fiber-matrix ITZ increases as the wall effect of the fibers decreases and their hydrophilicity increases (49). In Figures 12 (c) and 11 (b), dense hydration products (C-S-H gel or CH crystal group) are on the surface of BF and PF. The C-S-H gel accumulates on the fractured surface of BF and forms a relatively dense porous gel layer with residual alkali metal oxides. The result improves the bonding interface and mechanical interaction between fiber and cement matrix, increasing interface strength.

Figure 17 is an EDS point-scan. Si, Al, and S are on the fiber, so there may be C-S-H, AFt, or AFm. At point A, Ca/Si = 13.68, S/Ca = 0.01, which may be CH. Ca/Si = 0.15, S/Ca = 0.11 of point B. Moreover, Ca/Si = 1.38, S/Ca = 0.03 of point C should be C-S-H. The hydration products attached to the fiber improve the fiber-paste interaction force.

4. MECHANISM ANALYSIS

The shrinkage strain of concrete can lead to micro-cracks and pores between the concrete crystals, resulting in internal defects and decreased mechanical properties. This shrinkage will also be constrained by coarse aggregate and boundary conditions (47). The macroscopic properties of concrete are affected by the internal pore structure.

The hydration products, especially the C-S-H gel, filled the pores and blocked the pathways of capillary channels. Therefore, the presence of hydration products improves concrete compactness, bond strength, and mechanical friction between aggregates, and at the same time, will slow down the interfacial cracking. Ultimately, the interfacial transition zone and concrete matrix mechanical properties were enhanced (64). C-S-H accounts for about 70% of the fully hydrated cement paste, the primary source of cement strength. CH, which accounts for 20-25 %, has little effect on concrete, mainly in the aggregate cement interface transition zone, which is unfavorable to the bonding force and is the weak part.

Compared with NC, C-S-H increased, and CH decreased in BPHFRC. With the increase of fiber length, AFt and CH decrease, and the concrete becomes denser. This is due to the fiber-wrapped cement, which changes the direction and quantity of hydration products, decreasing the cracks and pores of aggregate cement ITZ.

The addition of fiber will affect the pore structure (25,65), energy absorption, and crack control of concrete. When the load is applied, the fiber undergoes pull out, fracture, friction slip, and debonding (55,66). Fiber orientation significantly affects the ability to absorb fracture energy and the mechanical properties of concrete (57,67). The opposite stress field is most effective when the fibers pass through the cracks vertically along the stress direction.

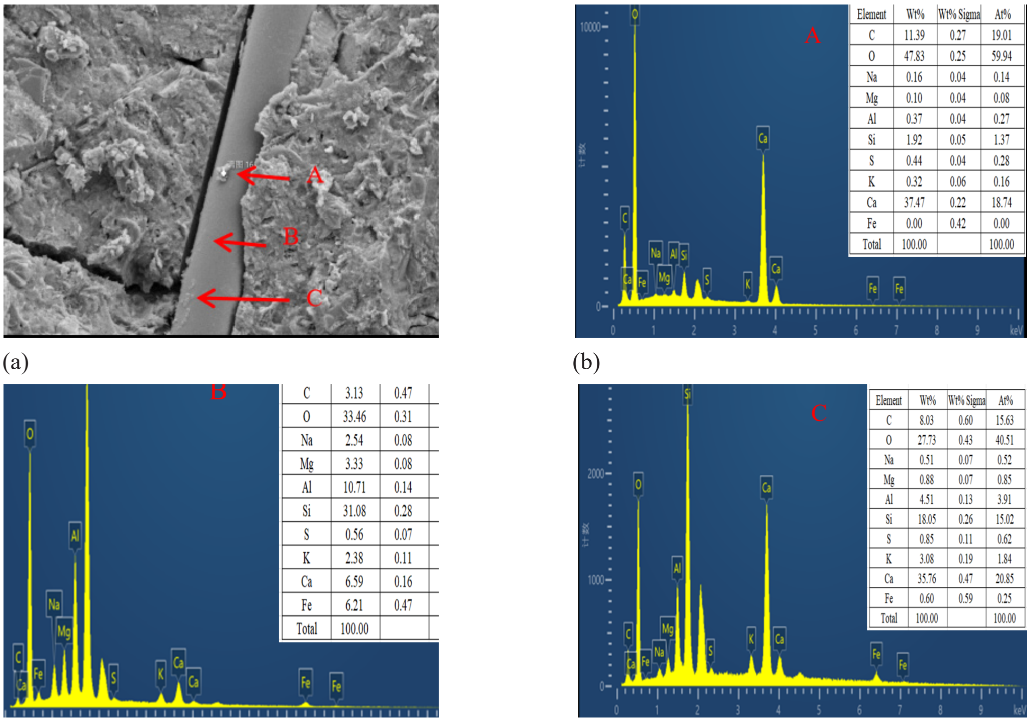

Figure 17. (a) SEM micrograph. (b) EDS Analysis of A. (c) EDS Analysis of B. (d) EDS Analysis of C.

Fracture of concrete occurs at the micro and macro levels, which is a gradual and multi-scale process. The schematic diagram of the crack resistance process at different zones by multi-scale hybrid fibers is illustrated in Figure 18. Concrete is loaded to the crack, and the damage process consists of a crack formation zone, a crack expansion zone, and a crack open zone. In the crack initiation stage, PF and BF cannot function due to the limitation of their large size. Only part of the BF provides resistance to microcracks. With further increase of applied load, the microcracks were transformed into mesocracks. At the stable crack propagation phase, BFs provide resistance to microscopic cracking. With the increased applied load, the PFs and partly the BFs resisted macrocracks during the unstable crack propagation phase. Constantly increasing loads eventually lead to fiber pull out or fracture and concrete failure.

In addition, hydrophilic BF has a strong bond with cement paste and a high modulus of elasticity. BF can form a load-bearing skeleton in concrete specimens, which can play a supportive role and inhibit the generation of microcracks, thus effectively improving crack resistance.

The spacing between PF and matrix increases with the shrinkage of concrete. Water molecules aggregate far away from PF to produce hydration products. The stacking structure of CH and AFt is loose, and the ITZ is weak. The low modulus of elasticity and high ductility of PF can inhibit the expansion of large cracks, effectively improving the toughness of concrete and preventing it from cracking. The large diameter of PF is more easily dispersed in concrete than BF (49), which can reduce the pores left in concrete due to the evaporation of water and effectively reduce the concentration of stress at the top of the pores. The high ductility of PF can counteract more tensile stresses through deformation and change the internal structure of concrete from the microscopic perspective. The use of more PFs results in higher tensile strength (50). PF with a low modulus of elasticity has a more significant effect on the splitting tensile strength of BPHFRC (53). The wall effect of a large diameter is significant. PF has a stronger wall effect than BF (49), which significantly impacts compressive strength. So, the PF content should not be too large for the compressive strength.

When the fiber content and L/D are too little, the fiber spacing is relatively large, and an effective three-dimensional network structure cannot be formed within the concrete. The effective bonding length of the fiber with the appropriate L/D ratio in the concrete matrix is longer than that of the small L/D ratio.

When the fiber content and L/D exceed the optimal range, folding and bending, uneven dispersion, aggregation, and bringing in air will occur, thus reducing compactness. At the same time, the fibers require more cement paste to wrap around, which tends to produce a large number of pores and interfacial bonding defects. It offsets the positive effect of the fiber part and produces negative effects, resulting in the fiber advantage not being fully utilized. It reduces fracture toughness and mechanical properties, which is not conducive to improving flexural tensile strength (66). The wall effect of long fiber is strong, which weakens the crack resistance and leads to a decrease in compressive strength. On the contrary, short fibers have a weak wall effect, preventing crack generation. Flexural strength is insensitive to the wall effect of long fibers compared to compressive strength. It does not fail to act as a crack resistant due to the fibers being parallel to the cracks.

Therefore, a proper L/D ratio has more excellent bonding and holding power compared to a too-small or too-large L/D ratio. It makes the concrete fracture toughness higher and can consume more energy to delay cracking effectively.

Fibers with different sizes and elastic moduli can play roles in restraining cracks at different stages of crack development, having a synergistic effect on improving the strength and deformation performance of the concrete. The synergistic effect of hybrid fibers combines the advantages of single fibers. The viscous effect and bridging crack resistance effect of the fibers can withstand the tensile force transmitted by the concrete matrix, inhibit the generation and expansion of cracks, and refine large cracks. The distribution of fibers in three dimensions changes the path of crack expansion, while the mechanism of fiber pull out transfers stress to the concrete matrix. It improves the bonding properties and internal integrity of the concrete. The elastic modulus and tensile strength of BPHFRC are much higher than those of PC. As a result, the tensile stress redistribution of the concrete ultimately improves the flexural and tensile capacity of the concrete. When the concrete cracks under pressure, the fibers bear the stress and restrain the lateral deformation of the concrete. Therefore, the volumetric strain and post-peak properties are improved, resulting in higher cubic and axial compressive strength.

From the energy point of view, concrete damage is caused by the internal load response caused by the external load reaching or exceeding its damage threshold. The more fibers there are, the larger the aspect ratio, and the higher the elastic modulus, the higher the energy consumption. After loading, NC only has a small amount of aggregate and inclusion cracks, which is a brittle failure. The loading time of BPHFRC is longer, and the crack can be completely extended. There is more debonding between aggregate and matrix, which causes more aggregate cracks and dissipates more energy. The damage is slow.

Therefore, the selection of fiber combination (A2B1C2) with appropriate content and L/D ratio could improve the cubic and axial compressive strengths. Whereas the selection of fiber combination (A2B2C3) could improve the splitting tensile and flexural strengths.

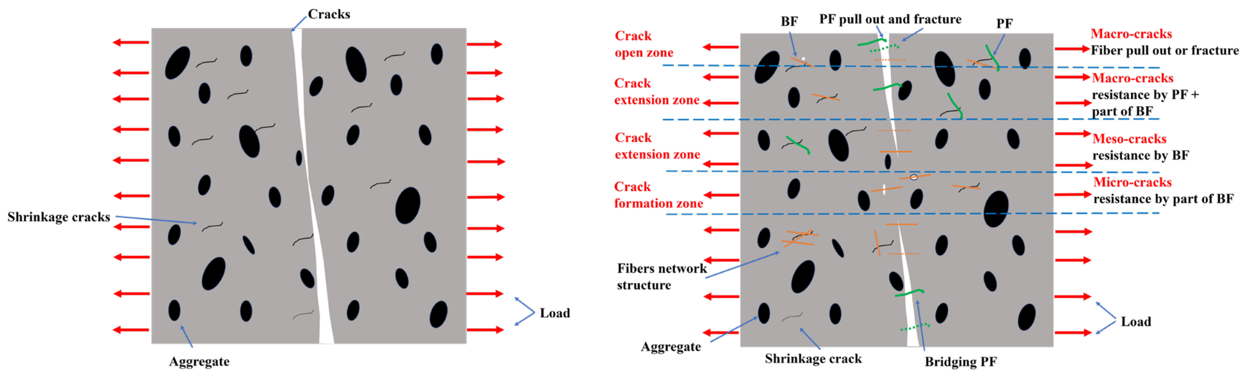

(a) (b)

Figure 18. Action mechanism of PC and HBPRC. (a) Crack of PC. (b) Crack resistance process at different zones by multi-scale hybrid fibers.

5. CONCLUSIONS

Based on the references (5, 6, 17, 68, 69), the effects of BFA and BFC/PFC are considered in this paper. Each combination has different crack suppression effects. The optimal combination of this paper is superior to the previous fiber content (BF: PF = 1:3), and the improvement of flexural strength is more prominent. Moreover, the compressive strength is better than others. This paper has discussed the mechanical properties and microstructure analysis of HBPFRC. The major conclusions of this study are listed below.

The BF and PF could significantly enhance the mechanical properties of BPHFRC. Test results indicated that the mechanical properties first increased and then decreased with the increase in the BFA. The optimum BFA is 800. The optimal combination for the test was A2B1C2, with relatively the best overall mechanical properties. The appropriate amount of L/D ratio and fiber content can better optimize the mechanical properties of hybrid fibers.

The influence of various factors on the cubic and axial compressive strengths of BPHFRC is BFC > BFA > PFC. The optimal combination of A2B1C2 (BFA of 800 (12 mm), BFC of 0.1, PFC of 0.15) increased cubic and axial compressive strengths by 13.73% and 23.54% compared to PC, with values of 47.22 MPa and 37.21 MPa, respectively.

A2B1C2 is a cost-effective and high-strength option for load-bearing construction, making it suitable for practical engineering applications.

Multiple factors impact the splitting tensile strength and flexural strength of BPHFRC, which is BFC > PFC > BFA. The optimal combination of A2B2C3 (BFA of 800 (12 mm), BFC of 0.15, PFC of 0.2) increased splitting tensile and flexural strengths by 32.96% and 38.88% compared to PC, with values of 4.72 MPa and 6.43 MPa, respectively. Polypropylene fiber is superior to basalt fiber in improving bending resistance and splitting tensile strength. In engineering practice, the optimal combination of A2B2C3 is preferred for bending members.

A prediction model of the mechanical properties of the BPHFRC was established considering the L/D ratio of BF, and the content of BF and PF. The paper presents a strength prediction model that can accurately predict the strength value of BPHFRC. The model has a relative error of less than 5.11%, making it highly reliable and valuable for practical applications.

The fiber toughening model includes the bridging and deflection of cracks and the pull out and fracture of fibers. The fiber L/D ratio and content of A2B1C2 and A2B2C3 are reasonable, which can achieve an excellent synergistic effect. SEM images of microstructure show that the BF bridges the initial micro-cracks and improves the tensile strength, while the PF bridges the macro-cracks and improves the ductility, the internal stress has been effectively exerted, and micro-cracks replace the main cracks. Thereby enhancing its mechanical properties. The hydration products make the concrete dense, improve the bite and bonding force of the interface between the aggregate, cement, and fiber, delay the crack initiation, and enhance the mechanical properties of the ITZ and the matrix.

Considering the practical application of BPHFC, the following aspects are worth studying. This paper only measured the mechanical properties, which have certain differences from the actual environment. Therefore, it is necessary to study the durability performance of BPHFRC further. The elastic modulus will be measured to analyze the post-peak failure of BPHFRC better. Other properties of concrete, such as fatigue resistance, will also be studied.

Acknowledgments

This work was supported by the Zhejiang Provincial Natural Science Foundation of China (Grant No. LQ22E080024), the Natural Science Foundation Project of Liaoning Provincial Department of Education, China (Grant No. JJL201915404), and the Zhejiang Province Department of Education Fund (Grant No. Y202146776). The authors are also thankful to Professor Huaxin Liu's research group for their help during the lab work. The careful review and constructive suggestions by the reviewers are gratefully acknowledged.

Funding sources

This work was supported by the Zhejiang Provincial Natural Science Foundation of China (Grant No. LQ22E080024), the Natural Science Foundation Project of Liaoning Provincial Department of Education, China (Grant No. JJL201915404), and the Zhejiang Province Department of Education Fund (Grant No. Y202146776).

Authorship contribution statement

Yuming Huang: Conceptualization, Formal analysis, Methodology, Validation, Visualization, Writing-original draft, Writing-review & editing.

Huaxin Liu: Data curation, Funding acquisition, Validation, Writing-review & editing.

Genjin Liu: Formal analysis, Funding acquisition, Writing-review & editing.

Declaration of competing interest

The authors of this article declare that they have no financial, professional or personal conflicts of in-terest that could have inappropriately influenced this work.

REFERENCES

1. Sozen MA, Ichinose T, Pujol S. 2014. Principles of reinforced concrete design (1st ed.). CRC Press. https://doi.org/10.1201/b17165
2. Habert G, Miller SA, John VM, Provis JL, Favier A, Horvath A, Scrivener KL. 2020. Environmental impacts and decarbonization strategies in the cement and concrete industries. Nat. Rev. Earth Environ. 1:559-573. https://doi.org/10.1038/s43017-020-0093-3

3. Zhao Y, Sun X, Cao P, Ling Y, Gao Z, Zhan Q, Zhou X, Diao M. 2019. Mechanical performance and numerical simulation of Basalt Fiber Reinforced Concrete (BFRC) using double-k fracture model and Virtual Crack Closure Technique (VCCT). Adv. Civ. Eng. 2019:1-15. https://doi.org/10.1155/2019/5630805
4. Wang. 1998. Toughness characteristics of synthetic fiber-reinforced cementitious composites. Fatigue Fract. Eng. Mat. Struct. 21(4):521-532. https://doi.org/10.1046/j.1460-2695.1998.00045.x
5. Fu Q, Xu W, Bu M, Guo B, Niu D. 2021. Effect and action mechanism of fibers on mechanical behavior of hybrid basalt-polypropylene fiber-reinforced concrete. Structures. 34:3596-3610. https://doi.org/10.1016/j.istruc.2021.09.097
6. Smarzewski P. 2019. Influence of basalt-polypropylene fibers on fracture properties of high performance concrete. Compos. Struct. 209:23-33. https://doi.org/10.1016/j.compstruct.2018.10.070
7. Chen R, Zhang G, Gu G. 2001. State of study and application of synthetic fibers reinforced concrete in China. J. Build. Mater. 2001(02):167-73.
8. Russo S, Silvestri M. 2008. Perspectives of employment of pultruded FRP structural elements in seismic engineering field. AIP Conf. Proc. American Institute of Physics. 1020:1103-1112. https://doi.org/10.1063/1.2963728
9. Shen K. 1998. The first composite long bridge in the world. Shanghai Building Materials. 1998(02):28-29.
10. Yazıcı Ş, İnan G, Tabak V. 2007. Effect of aspect ratio and volume fraction of steel fiber on the mechanical properties of SFRC. Constr. Build. Mater. 21(6):1250-1253. https://doi.org/10.1016/j.conbuildmat.2006.05.025
11. Afroughsabet V, Biolzi L, Ozbakkaloglu T. 2016. High-performance fiber-reinforced concrete: a review. J. Mater. Sci. 51:6517-6551. https://doi.org/10.1007/s10853-016-9917-4
12. Deng M, Zhang M, Zhu Z, Ma F. 2021. Deformation capacity of over-reinforced concrete beams strengthened with highly ductile fiber-reinforced concrete. Structures. 29:1861-1873. https://doi.org/10.1016/j.istruc.2020.12.062
13. Ganta JK, Seshagiri Rao MV, Mousavi SS, Srinivasa Reddy V, Bhojaraju C. 2020. Hybrid steel/glass fiber-reinforced self-consolidating concrete considering packing factor: Mechanical and durability characteristics. Structures. 28:956-972. https://doi.org/10.1016/j.istruc.2020.09.042
14. Sivakumar A, Santhanam M. 2007. Mechanical properties of high strength concrete reinforced with metallic and non-metallic fibers. Cem. Concr. Compos. 29(8):603-608. https://doi.org/10.1016/j.cemconcomp.2007.03.006
15. Geng Y, Leung CKY. 1996. A microstructural study of fiber/mortar interfaces during fiber debonding and pull-out. J. Mater. Sci. 31:1285-1294. https://doi.org/10.1007/BF00353108
16. Brandt AM. 1985. On the optimal direction of short metal fibers in brittle matrix composites. J. Mater. Sci. 20:3831-3841. https://doi.org/10.1007/BF00552371
17. Khan M, Cao M, Ali M. 2020. Cracking behaviour and constitutive modelling of hybrid fiber reinforced concrete. J. Build. Eng. 30:101272. https://doi.org/10.1016/j.jobe.2020.101272
18. Ahmed TW, Aljubory NH, Zidan RS. 2021. Properties and performance of polypropylene fiber reinforced concrete: A review. Tikrit J. Eng. Sci. 27(2):82-97. https://doi.org/10.25130/tjes.27.2.10
19. Banthia N, Majdzadeh F, Wu J, Bindiganavile V. 2014. Fiber synergy in Hybrid Fiber Reinforced Concrete (HyFRC) in flexure and direct shear. Cem. Concr. Compos. 48:91-97. https://doi.org/10.1016/j.cemconcomp.2013.10.018
20. Wang D, Ju Y, Shen H, Xu L. 2019. Mechanical properties of high performance concrete reinforced with basalt fiber and polypropylene fiber. Constr. Build. Mater. 197:464-473. https://doi.org/10.1016/j.conbuildmat.2018.11.181
21. Rooholamini H, Hassani A, Aliha MRM. 2018. Fracture properties of hybrid fiber-reinforced roller-compacted concrete in mode I with consideration of possible kinked crack. Constr. Build. Mater. 187:248-256. https://doi.org/10.1016/j.conbuildmat.2018.07.177
22. Khan M, Cao M. 2021. Effect of hybrid basalt fiber length and content on properties of cementitious composites. Mag. Concr. Res. 73(10):487-498. https://doi.org/10.1680/jmacr.19.00226
23. Marcos-Meson V, Michel A, Solgaard A, Fischer G, Edvardsen C, Skovhus TL. 2018. Corrosion resistance of steel fiber reinforced concrete - A literature review. Cem. Concr. Res. 103:1-20. https://doi.org/10.1016/j.cemconres.2017.05.016
24. Jiang C, Fan K, Wu F, Chen D. 2014. Experimental study on the mechanical properties and microstructure of chopped basalt fiber reinforced concrete. Mater. Des. 58:187-193. https://doi.org/10.1016/j.matdes.2014.01.056
25. Sim J, Park C, Moon DY. 2005. Characteristics of basalt fiber as a strengthening material for concrete structures. Compos. B. Eng. 36(6-7):504-512. https://doi.org/10.1016/j.compositesb.2005.02.002
26. Zhang X, Gu X, Lv J. 2018. Effect of basalt fiber distribution on the flexural–tensile rheological performance of asphalt mortar. Constr. Build. Mater. 179:307-314. https://doi.org/10.1016/j.conbuildmat.2018.05.089
27. Huo J, Lei Y, Wang H, Liu S. 2006. Progress of study on the preparation of basalt fibet and composite material of basalt fiber. Mater. Rep. 1:382-385.
28. Zhang X, Qin W, Tian Q, Wang F, Fan Y. 2018. Research progress of the material properties on basalt fiber reinforced concrete. Concrete. 2:94-97. https://doi.org/10.3969/j.issn.1002-3550.2018.02.026
29. He W, Chen S, Zhang X. 2013. Study on progress of polypropylene fiber reinforced concrete. New Chem. Mater. 41(03):130-132.
30. Kabay N. 2014. Abrasion resistance and fracture energy of concretes with basalt fiber. Constr. Build. Mater. 50:95-101. https://doi.org/10.1016/j.conbuildmat.2013.09.040
31. Algin Z, Ozen M. 2018. The properties of chopped basalt fiber reinforced self-compacting concrete. Constr. Build. Mater. 186:678-685. https://doi.org/10.1016/j.conbuildmat.2018.07.089

32. Lv X, Xue G, Zhong X. 2021. Influence of basalt fiber length-diameter ratio on the mechanical properties of concrete. Journal of Shijiazhuang Institute of Railway Technology. 20(01):67-72.
33. Kizilkanat AB, Kabay N, Akyüncü V, Chowdhury S, Akça AH. 2015. Mechanical properties and fracture behavior of basalt and glass fiber reinforced concrete: An experimental study. Constr. Build. Mater. 100:218-224. https://doi.org/10.1016/j.conbuildmat.2015.10.006
34. Arslan ME. 2016. Effects of basalt and glass chopped fibers addition on fracture energy and mechanical properties of ordinary concrete: CMOD measurement. Constr. Build. Mater. 114:383-391. https://doi.org/10.1016/j.conbuildmat.2016.03.176
35. Khan M, Cao M, Xie C. 2021. Ali M. Efficiency of basalt fiber length and content on mechanical and microstructural properties of hybrid fiber concrete. Fatigue Fract. Eng. Mat. Struct. 44(8):2135-2152. https://doi.org/10.1111/ffe.13483
36. Zhu H, Yan M, Wang P, Li C, Cheng Y. 2015. Mechanical performance of concrete combined with a novel high strength organic fiber. Constr. Build. Mater. 78:289-294. https://doi.org/10.1016/j.conbuildmat.2015.01.014
37. Luo H, Yang D, Zhou X, Shan C, Liu X, Zhao F. 2019. Mechanical properties of polypropylene fiber reinforced concrete with different aspect ratios. Acta Materiae Compositae Sinica. 36(08):1935-1948. https://doi.org/10.13801/j.cnki.fhclxb.20180917.001
38. He W, Kong X, Gao H, Liu H, Wang X. 2020. Research on the mechanical properties and microstructure of recycled aggregate concrete with high content polypropylene fiber. Concrete. 1:82-86. https://doi.org/10.3969/j.issn.1002-3550.2020.01.019
39. Shi F, Pham TM, Hao H, Hao Y. 2020. Post-cracking behaviour of basalt and macro polypropylene hybrid fiber reinforced concrete with different compressive strengths. Constr. Build. Mater. 262:120108. https://doi.org/10.1016/j.conbuildmat.2020.120108
40. Huang D, Niu D, Liu H, Su L, Xia Q. 2023. Mechanical Properties, Permeability and Pore Structure of Basalt-Polypropylene Fiber Reinforced Concrete. Journal of Yangtze River Scientific Research Institute. 40(2):147-152. https://doi.org/10.11988/ckyyb.20211046
41. Mu R, Li H, Qing L, Lin J, Zhao Q. 2017. Aligning steel fibers in cement mortar using electro-magnetic field. Constr. Build. Mater. 131:309-316. https://doi.org/10.1016/j.conbuildmat.2016.11.081
42. Afroz M, Patnaikuni I, Venkatesan S. 2017. Chemical durability and performance of modified basalt fiber in concrete medium. Constr. Build. Mater. 154:191-203. https://doi.org/10.1016/j.conbuildmat.2017.07.153
43. GB/T50081-2019. 2019. Standard for test methods of concrete physical and mechanical properties. China Stand.
44. Wang J, Zheng C, Jin B, Zhao Y, Li S, Li X, Yang B, Hou Y. 2022. Effect of fly ash/different aggregates on the mechanical properties of fiber reinforced self-compacting recycled concrete. J. Funct. Mater. 53(9):9209-9218. https://doi.org/10.3969/j.issn.1001-9731.2022.09.030
45. Shi Y, Liu L, Chen G. 2023. Experimental study on mechanical properties of polypropylene fiber ceramsite concrete. China Measurement & Test. 49(9):167-173. https://doi.org/10.11857/j.issn.1674-5124.2022050123
46. Ding W, Leng F, Zhao W. 2007. Analysis on concrete water consumption standard JGJ63-2006. Constr. Technol. 36(4):92-93.
47. Xiang P. 2022. Experimental study on mechanical properties of steel-jute hybrid fiber concrete. AnHui University of Science and Technology. https://doi.org/10.26918/d.cnki.ghngc.2022.000650
48. Toutanji, HA. 1999. Properties of polypropylene fiber reinforced silica fume expansive-cement concrete. Constr. Build. Mater. 13(4):171-177. https://doi.org/10.1016/S0950-0618(99)00027-6
49. Li D, Niu D, Fu Q, Luo D. 2020. Fractal characteristics of pore structure of hybrid basalt–polypropylene fibre-reinforced concrete. Cem. Concr. Compos. 109:103555. https://doi.org/10.1016/j.cemconcomp.2020.103555
50. Smarzewski P. 2019. Influence of basalt-polypropylene fibres on fracture properties of high performance concrete. Compos. Struct. 209:23-33. https://doi.org/10.1016/j.compstruct.2018.10.070
51. Ranjbar N, Talebian S, Mehrali M, Kuenzel C, Cornelis Metselaar HS, Jumaat MZ. 2016. Mechanisms of interfacial bond in steel and polypropylene fiber reinforced geopolymer composites. Compos. Sci. Technol. 122:73-81. https://doi.org/10.1016/j.compscitech.2015.11.009
52. Lou K, Xiao P, Wu B, Kang A, Wu X, Shen Q. 2021. Effects of fiber length and content on the performance of ultra-thin wearing course modified by basalt fibers. Constr. Build. Mater. 313:125439. https://doi.org/10.1016/j.conbuildmat.2021.125439
53. Wang D, Ju Y, Shen H, Xu L. 2019. Mechanical properties of high performance concrete reinforced with basalt fiber and polypropylene fiber. Constr. Build. Mater. 197:464-473. https://doi.org/10.1016/j.conbuildmat.2018.11.181
54. Jiang C, Fan K, Wu F, Chen D. 2014. Experimental study on the mechanical properties and microstructure of chopped basalt fibre reinforced concrete. Mater. Des. 58:187-193. https://doi.org/10.1016/j.matdes.2014.01.056
55. Yang S, Gao D, Zhao J. 2010. Microstructure of fiber reinforced concrete with slag power after effect of high temperatures. Journal of Southeast University (Natural Science Edition). 40(S2):102-106.
56. Liu Z, Chen X, Han Z, Han X, Jin X. 2019. Study on the influence of pore structure on the mechanical properties of basalt fiber reinforced concrete. China Concrete and Cement Products. 1:47-50. https://doi.org/10.19761/j.1000-4637.2019.01.047.04
57. Harrisson AM, Winter NB. Taylor, HFW. 1987. X-ray microanalysis of microporous materials. J. Mater. Sci. Lett. 6:1339-1340. https://doi.org/10.1007/BF01794611
58. Card JA, Mohan K, Taylor HFW, Cliff G. 2006. Analytical electron microscopy of cement pastes: I, tricalcium silicate pastes. J. Am. Ceram. Soc. 63(5-6):336-337. https://doi.org/10.1111/j.1151-2916.1980.tb10733.x
59. Zhu S. 2020. Study on the interfacial transition zone feature and improving mechanical properties of Rubber concrete with waste tires. China University of Mining and Technology. https://doi.org/10.27623/d.cnki.gzkyu.2020.001447
60. Mo L, Deng M, Tang M, Al-Tabbaa A. 2014. MgO expansive cement and concrete in China: Past, present and future. Cem. Concr. Res. 57:1-12. https://doi.org/10.1016/j.cemconres.2013.12.007

61. Wang J, Niu D, He H, Wang B. 2019. Durability degradation of lining shotcrete exposed to compound salt. China Civ. Eng. J. 52(09):79-90. https://doi.org/10.15951/j.tmgcxb.2019.09.006
62. Zhang C. 2020. Analysis of the effect of water on the mechanical properties of polypropylene fiber reinforced concrete. Harbin Engineering University. https://doi.org/10.27060/d.cnki.ghbcu.2020.001479
63. Sui H. 2024. Research on mechanical properties and microstructure of fiber reinforced concrete. Heilongjiang University. https://doi.org/10.27123/d.cnki.ghlju.2024.001298
64. Huang W, Zhang Y, Ge J, Fang Z. 2022. Experimental study and microscopic analysis of the mechanical properties of basalt fiber and nano-SiO2 reinforced concrete. China Concrete and Cement Products. 04:55-58. https://doi.org/10.19761/j.1000-4637.2022.04.055.05
65. Larsen IL, Thorstensen RT. 2020. The influence of steel fibers on compressive and tensile strength of ultra high performance concrete: A review. Constr. Build. Mater. 256:119459. https://doi.org/10.1016/j.conbuildmat.2020.119459
66. Wuest J, Denarié E, Brühwiler E, Tamarit L, Kocher M, Gallucci E. 2009. Tomography analysis of fiber distribution and orientation in ultra high–performance fiber-reinforced composites with high-fiber dosages. Exp. Tech. 33(5):50-55. https://doi.org/10.1111/j.1747-1567.2008.00420.x
67. Stähli P, Custer R, Van Mier JGM. 2008. On flow properties, fiber distribution, fiber orientation and flexural behaviour of FRC. Mater. Struct. 41:189-196. https://doi.org/10.1617/s11527-007-9229-x
68. Yao Y, Wang B, Zhuge Y, Huang Z. 2022. Properties of hybrid basalt-polypropylene fiber reinforced mortar at different temperatures. Constr. Build. Mater. 346:128433. https://doi.org/10.1016/j.conbuildmat.2022.128433
69. Zhang Y, Sun X. 2023. An investigation of the hybrid effect of pre-absorbed lightweight aggregate and basalt-polypropylene fiber on concrete performance. Constr. Build. Mater. 408:133626. https://doi.org/10.1016/j.conbuildmat.2023.133626